Mon. Not. R. Astron. Soc. **000**, 1–14 (2011) Printed 24 October 2011 (MN LATEX style file v2.2)

A simplified view of blazars: clearing the fog around long-standing selection effects

P. Giommi[1⋆], P. Padovani[2], G. Polenta[1,3], S. Turriziani[1], V. D'Elia[1,3], S. Piranomonte[3]

[1] *ASI Science Data Center, c/o ESRIN, via G. Galilei, 00044 Frascati, Italy*
[2] *European Southern Observatory, Karl-Schwarzschild-Str. 2, D-85748 Garching bei München, Germany*
[3] *INAF-Osservatorio Astronomico di Roma, via Frascati 33, I-00040 Monteporzio Catone, Italy*

Accepted 2011 October 20. Received 2011 October 4; in original form 2011 July 13

ABSTRACT

We propose a scenario where blazars are classified as flat-spectrum radio quasars (FSRQs), BL Lacs, low synchrotron, or high synchrotron peaked objects according to a varying mix of the Doppler boosted radiation from the jet, the emission from the accretion disk, the broad line region, and the light from the host galaxy. In this framework the peak energy of the synchrotron power ($\nu^S_{\rm peak}$) in blazars is independent of source type and of radio luminosity. We test this new approach, which builds upon unified schemes, using extensive Monte Carlo simulations and show that it can provide simple answers to a number of long-standing issues including, amongst others, the different cosmological evolution of BL Lacs selected in the radio and X-ray bands, the larger $\nu^S_{\rm peak}$ values observed in BL Lacs, the fact that high synchrotron peaked blazars are always of the BL Lac type, and the existence of FSRQ/BL Lac transition objects. Objects so far classified as BL Lacs on the basis of their *observed* weak, or undetectable, emission lines are of two physically different classes: intrinsically weak lined objects, more common in X-ray selected samples, and heavily diluted broad lined sources, more frequent in radio selected samples, which explains some of the confusion in the literature. We also show that strong selection effects are the main cause of the diversity observed in radio and X-ray samples, and that the correlation between luminosity and $\nu^S_{\rm peak}$, that led to the proposal of the "blazar sequence", is also a selection effect arising from the comparison of shallow radio and X-ray surveys, and to the fact that high $\nu^S_{\rm peak}$ - high radio power objects have never been considered because their redshift is not measurable.

Key words: BL Lacertae objects: general — quasars: emission lines — radiation mechanisms: non-thermal — radio continuum: galaxies — X-rays: galaxies

1 INTRODUCTION

Once considered rare sources, blazars, a type of radio loud active galactic nuclei (AGN) pointing their jets in the direction of the observer (see e.g. Blandford & Rees 1978; Urry & Padovani 1995), are now being detected in increasingly larger numbers. Recent results from the *Wilkinson Microwave Anisotropy Probe* (WMAP), the *Planck* and *Fermi* satellites have established that blazars are the most common type of extragalactic sources found at microwave and γ-ray energies (Giommi et al. 2007; Abdo et al. 2010a; Planck Collaboration 2011). So far about 3,000 blazars are known (Massaro et al. 2009, 2011), but their number is steadily growing thanks to the *Fermi* (Abdo et al. 2010b, 2011), the optical Sloan Digital Sky Survey (SDSS: Plotkin et al. 2010), and the *Planck* (Planck Collaboration 2011) surveys. Some faint blazars are also being detected as serendipitous sources in *Swift*-XRT images (Turriziani 2010, 2011).

While all blazars share the same property of emitting variable, non-thermal radiation across the entire electromagnetic spectrum, they also display diversity. Namely, they come in two main subclasses, whose major difference is in their optical properties: 1) Flat Spectrum Radio Quasars (FSRQs), which show strong, broad emission lines in their optical spectrum, just like radio quiet QSOs;

⋆ E-mail: paolo.giommi@asdc.asi.it

and 2) BL Lacs, which are instead characterized by an optical spectrum, which at most shows weak emission lines, sometimes displays absorption features, and in some cases can be completely featureless. Historically, the separation between BL Lacs and FSRQs has been made at the (rather arbitrary) rest-frame equivalent width (EW) of 5 Å (e.g. Stickel et al. 1991; Stocke et al. 1991). However, no evidence for a bimodal distribution in the EW of the broad lines of radio quasars has ever been found and, on the contrary, Scarpa & Falomo (1997) pointed out that radio-selected BL Lacs were, from the point of view of the emission line properties, very similar to FSRQs but with a stronger continuum. Most BL Lacs selected in the X-ray band, on the other hand, had very weak, if any, emission lines, and Stocke et al. (1991), when studying the properties of the X-ray selected *Einstein* Medium Sensitivity Survey (EMSS) sample, had to introduce another criterion to identify BL Lacs, this time to separate them from galaxies. This was based on the Ca H&K break, a stellar absorption feature typically found in the spectra of elliptical galaxies. Given that its value in non-active ellipticals is $\sim 50\%$, Stocke et al. (1991) chose a maximum value of 25% to ensure the presence of a substantial non-thermal continuum superposed to the host galaxy spectrum. This was later revised to 40% (Marchã et al. 1996; Landt, Padovani, & Giommi 2002).

Blazar classification depends then on the details of their appearance in the optical band where they emit a mix of three types of radiation: 1) a non-thermal, jet-related, component; 2) thermal radiation coming from the accretion onto the supermassive black hole and from the broad line region (at least in most radio-selected sources); 3) light from the host (giant elliptical) galaxy. Figure 1 represents these three components as red, blue and orange lines, overlaid to the spectral energy distribution (SED) of four well-known blazars (from Giommi et al. 2011). The strong non-thermal radiation, the only one that spans the entire electromagnetic spectrum, is composed of two basic parts forming two broad humps, the low-energy one attributed to synchrotron radiation, and the high-energy one, usually thought to be due to inverse Compton radiation (see e.g. Abdo et al. 2010c). The peak of the synchrotron hump ($\nu^S_{\rm peak}$) can occur at different frequencies, ranging from about $\sim 10^{12.5}$ Hz to over 10^{18} Hz (see e.g. the cases of 3C 273 or 3C 279 and MKN 501 in Fig. 1) reflecting the maximum energy at which particles can be accelerated (e.g. Giommi et al. 2011). Blazars where $\nu^S_{\rm peak}$ is lower than 10^{14} Hz in their rest frame are called Low Synchrotron Peaked (LSP) sources, while those where 10^{14} Hz $< \nu^S_{\rm peak} < 10^{15}$ Hz, and $\nu^S_{\rm peak} > 10^{15}$ Hz are called Intermediate and High Synchrotron Peaked (ISP and HSP) sources respectively (Abdo et al. 2010c). This definition extends the original division of BL Lacs into LBL and HBL sources first introduced by Padovani & Giommi (1995).

The large $\nu^S_{\rm peak}$ disparity between LSP and HSP blazars (up to five orders of magnitude) is the cause of very large differences between the intensity of the radiation emitted in different energy bands. For instance, for the same radio flux an HSP source can be a factor of a 100 brighter in the optical band, or even a factor of a 1,000 brighter in the X-ray band, than an LSP blazar. This induces very strong selection effects in blazar samples discovered in different bands and led to some confusion when comparing, for example, the first radio and X-ray-selected BL Lac samples in the early 1990's.

We feel that all the above factors, which play an important role in blazar classification, have not been properly taken into account so far. The purpose of this paper is then to propose a new hypothesis to explain the existence of apparently different properties of the blazar subclasses, which solves at once many of the open issues of blazar research.

Throughout this paper we use a ΛCDM cosmology with $H_0 = 70$ km s^{-1} Mpc^{-1}, $\Omega_m = 0.27$ and $\Omega_\Lambda = 0.73$ (Komatsu et al. 2011).

2 CURRENT STATUS: TWO TYPES OF BLAZAR POPULATIONS WITH WIDELY DIFFERENT PROPERTIES

The two main blazar subclasses have many differences, which include:

(i) *different optical spectra* (by definition). There are, however, a number of BL Lac - FSRQ transition objects, which include even BL Lacertae itself, the prototype of the class, which displays at times moderately strong, broad lines (e.g. Vermeulen et al. 1996; Capetti et al. 2010; Ghisellini et al. 2011) and 3C 279, a well-studied FSRQ, which can appear nearly featureless in a bright state (Pian et al. 1999);

(ii) *different extended radio powers.* Most BL Lacs have extended radio powers and morphologies consistent with those of Fanaroff-Riley (FR) type I, while basically all FSRQs are FR II-like (Urry & Padovani 1995, and references therein). However, despite the difficulty of classifying the radio morphology of sources with their jets forming a small angle with respect to the line of sight, some radio-selected BL Lacs are known to posses an FR II-like structure (e.g. Kollgaard et al. 1992; Rector & Stocke 2001);

(iii) *very different redshift distributions.* FSRQs, similarly to radio quiet QSOs, are typically found at redshifts $\sim 1-2$, and up to ~ 5.5, while BL Lacs are usually much closer with very few cases at $z \gtrsim 0.6$. This is graphically shown in Fig. 2, which plots the redshift distribution of all the FSRQs and BL Lacs included in the third edition of BZCAT (Massaro et al. 2009, 2011), the largest compilation of blazars currently available. It must be stressed, however, that a large fraction of BL Lacs ($\sim 43\%$ in BZCAT and $> 50-60\%$ of the BL Lacs in the Fermi 1 and 2 year AGN catalogs: Abdo et al. 2010a, 2011b) have no measured redshift, due to the lack of any detectable feature in their optical spectrum, despite the use of 10-m class optical telescopes for the spectroscopy identification campaign (Shaw et al. 2009, 2010);

(iv) *different cosmological evolutions.* Detailed analyses of both radio selected and X-ray selected samples have led to the conclusion that the cosmological evolution of the two blazar subclasses are very different, with FSRQs evolving strongly (again similarly to ra-

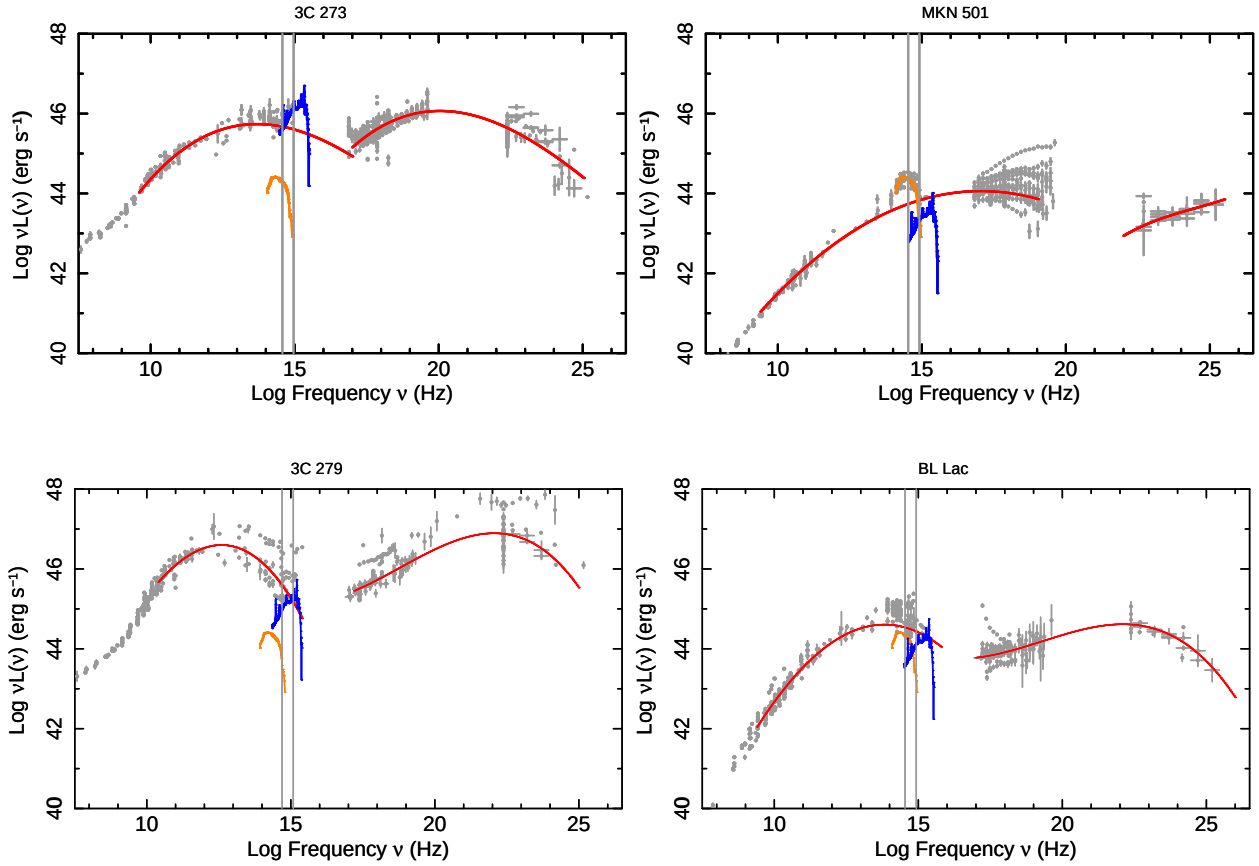

Figure 1. The SEDs of four representative blazars: two FSRQs, 3C 273 and 3C 279, and two BL Lacs, MKN 501 and BL Lac. The lines in color denote the three main components of blazars SEDs, namely non-thermal radiation from the jet (red), emission from the disk and from the broad line region represented by the composite QSO optical spectrum of Vanden Berk et al. (2001) (blue), and light from the host galaxy, represented by the giant elliptical template of Mannucci et al. (2001) (orange). The two vertical lines indicate the optical observing window ($3800 - 8000$ Å). See text for details.

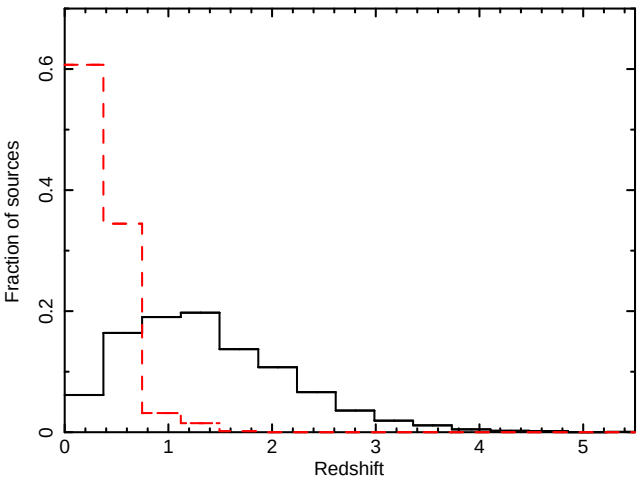

Figure 2. The redshift distribution of FSRQs (1676 objects, solid line) and BL Lacs (537 objects, dashed line) in the third edition of the BZCAT catalogue (Massaro et al. 2009, 2011). The two distributions are obviously different at the > 99.99 level, with means of 1.4 and 0.36 respectively. About 400 BL Lacs with no redshift determination in the BZCAT catalogue have been excluded.

dio quiet QSOs) and BL Lacs evolving at a similar, or perhaps lower rate, in the radio band, or even showing no or negative evolution in the X-ray band (e.g. Stickel et al. 1991; Giommi, Menna & Padovani 1999; Rector et al. 2000; Beckmann et al. 2003; Padovani et al. 2007; Giommi et al. 2009, and references therein);

(v) *widely different mix of FSRQs and BL Lacs in radio and X-ray selected samples*, with the latter typically including a much larger fraction of BL Lacs than the former. In fact, while only $\sim 15\%$ of WMAP5 blazars are BL Lacs (Section 4.1), this fraction is instead $\sim 70\%$ in the EMSS complete sample, which includes 41 BL Lacs and 15 FSRQs (Rector et al. 2000; Padovani et al. 2003);

(vi) *widely different distributions of the synchrotron peak energy* $\nu^S_{\rm peak}$. The rest-frame $\nu^S_{\rm peak}$ distribution of FSRQs is strongly peaked at low energies ($\langle \nu^S_{\rm peak} \rangle = 10^{13.1\pm0.1}$ Hz) and never reaches very high values ($\nu^S_{\rm peak} \lesssim 10^{14.5}$ Hz) independently of the selection method (Giommi et al. 2011), while the $\nu^S_{\rm peak}$ distribution of BL Lacs is shifted to higher values by at least one order of magnitude. It can also reach values as high as $\nu^S_{\rm peak} \gtrsim 10^{18}$ Hz and its shape varies strongly depending on the selection band (that is radio, X-ray or γ-ray: Abdo et al. 2010c; Giommi et al. 2011).

Some of these differences have been explained by so-called unified schemes, which posit that BL Lacs and FSRQs are simply FR I and FR II radio galaxies with their jets forming a small angle with respect to the line of sight (Urry & Padovani 1995). (Radio galaxies would then be the "parent" population of blazars). Due to relativistic beaming this has enormous effects on their apparent emitted power and luminosity functions (LFs) and can explain their different extended radio powers and, partly, their cosmological evolutions. However, unified schemes per se cannot account for transition objects, and the different evolution of radio and X-ray selected BL Lacs and $\nu^S_{\rm peak}$ distributions. Our new hypothesis builds upon unified schemes by adding dilution and strong selection effects as new, vital components.

3 THE EW OF FSRQS AND RADIO QUIET QSOS

The existence of BL Lac - FSRQ transition objects and the recent finding that unresolved radio quasars (i.e. FSRQs) appear to be redder than radio quiet AGN (Kimball et al. 2011) suggest that the strong non-thermal jet emission in blazars may have a significant impact on the shape of their blue bump and on the EW of their broad lines. In particular, given this extra continuum component, the EWs of broad-lined blazars (FSRQs) should be systematically lower than those of radio-quiet AGN.

To test this, we extracted EW data for samples of radio-quiet QSOs and blazars from the SDSS DR-7 spectral database. In order to have a sample that is not excessively large but still representative of the entire data set, we considered only radio-quiet QSOs with $28^\circ \leqslant b_{\rm II} \leqslant 30^\circ$, thus limiting the sample size to about 650 sources. To obtain the EW of a sizable sample of blazars we considered all FSRQs in BZCAT with 1.4 GHz flux > 300 mJy (to simulate a radio flux-limited sample) and in the WMAP5 catalogue. For each object in the three samples we retrieved, from the SDSS on-line system, the line measurements parameters (e.g. EW, χ^2_ν of the fit etc.) of the strongest emission lines in quasar spectra, that is Lyα, C IV, C III, Mg II, Hβ, Hα. Details on the fitting algorithm can be found at the SDSS website[1]. To avoid problematic cases, for our analysis we considered only SDSS fits to emission lines with $\chi^2_\nu \leqslant 2.5$.

Figure 3 shows the distribution of the EW of the MgII emission line, for which we have better statistics, for the sample of radio quiet SDSS QSOs (663 objects), BZCAT (126 objects) and WMAP5 (35 objects) FSRQs. The EW of both blazar samples is smaller than that of radio quiet QSOs, with median values respectively equal to 16.4 (BZCAT), 14 (WMAP5), and 18.4 Å (radio-quiet QSOs). A Kolmogorov-Smirnov (KS) test gives a probability $< 0.1\%$ that both FSRQ samples have the same distribution as that of radio-quiet AGN. Moreover, we found that this dilution increases further (i.e. the median EW gets smaller) if we make a cut at higher radio fluxes

[1] http://www.sdss.org/dr7/algorithms/speclinefits.html

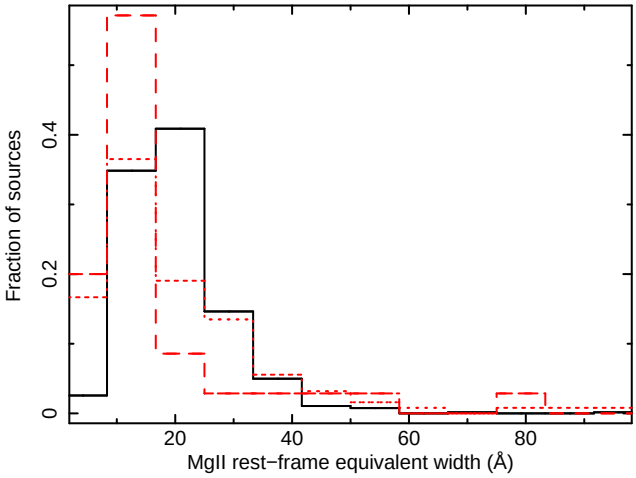

Figure 3. The distribution of the Mg II rest-frame EW for a sample of 663 radio quiet quasars (solid histogram) compared to the distributions of the Mg II EW of 35 WMAP5 and 126 FSRQs in BZCAT (dashed and dotted histograms respectively) with SDSS-DR7 spectrum and $\chi^2_\nu \leqslant 2.5$. The blazar EW distribution is significantly shifted towards lower values compared to radio quiet QSOs. See text for details.

in the BZCAT FSRQs. Similar results were obtained for the other emission lines. This demonstrates that the broad lines of blazars are significantly diluted compared to those of radio quiet QSOs. The mean absolute magnitudes of the blazar and radio-quiet samples agree within ~ 0.2 magnitudes, which means that the difference cannot be due to the well-known anti-correlation between EW and absolute magnitude, the so-called "Baldwin effect" (Baldwin 1977).

We note that a number of papers have stated that the optical spectra of radio-quiet and radio-loud QSOs are not significantly different (e.g. Francis et al. 1993, and references therein). However, the radio-loud samples on which this conclusion was based were still optically selected and required the presence of a UV excess and/or strong emission lines. Therefore, these radio-loud samples were biased towards objects with strong blue bumps.

4 A NEW, MUCH SIMPLER, SCENARIO FOR BLAZARS

The considerations made in the previous sections lead us to propose a new, very simple scenario where the observed blazar optical spectrum is the result of a combination of an intrinsic EW distribution and the effects of three components: a non-thermal, jet related one, a thermal one due to the accretion disk, and emission from the host galaxy. Different mixes of these components determine the appearance of the optical spectrum and therefore the classification of sources in FSRQs (dominated by strong lines), BL Lacs (with diluted, weak lines, if a standard accretion disk is present), and radio-galaxies (where the host galaxy swamps both the thermal and non-thermal nuclear emission present in blazars). The other novel component is a single LF whose evolution

depends on radio power. This idea was tested through extensive Monte Carlo simulations, as described below.

4.1 Simulation ingredients

Our simulations include the following ingredients, which we kept as simple as possible and tied as much as possible to observational data:

(i) **Luminosity function** We derive the LF and evolution of blazars at 41 GHz from the Wilkinson Microwave Anisotropy Probe (WMAP5) sample (Wright et al. 2009). Given that the mean blazar radio - sub-mm spectral index is ~ 0 (Giommi et al. 2009) this is practically equivalent to a radio-selected sample. We extend on the work of Giommi et al. (2009), which was based on WMAP3, and define a flux-limited sample of high Galactic latitude sources ($f_{41GHz} \geqslant 0.9$ Jy, $|b_{\rm II}| > 15^{\circ}$) including 161 FSRQs, 29 BL Lacs, and 10 blazars of unknown type. By applying a maximum likelihood technique to the WMAP5 blazars (see, e.g. Padovani et al. 2011, for details) we obtain, together with the evolution discussed below, a best-fit local LF $\Phi(P) \propto P^{-3}$ (in units of Gpc^{-3} P^{-1}) between 1.9×10^{24} and 4.2×10^{27} W/Hz, which we assume in our radio simulations.

(ii) **Cosmological evolution** Powerful ($P_{\rm r} \gtrsim 10^{26}$ W/Hz) radio sources are known to display a strong, positive evolution at moderately low redshifts followed by a decline at higher redshifts (e.g. Wall et al. 2005, and references therein). We parametrize this behaviour with a simple model of the type $P(z) = (1+z)^{k+\beta z}$, which allows for a maximum in the luminosity evolution followed by a decline. This was first suggested by Wall, Pope & Scott (2008) and applied by Ajello et al. (2009) to a sample of *Swift*/BAT blazars. A maximum likelihood technique applied to the WMAP5 blazar sample allows us to derive $k = 7.3$ and $\beta = -1.5$ in the $0-3.4$ redshift range (which implies a peak at $z \sim 1.85$), which we assume in our simulations. The case of pure luminosity evolution ($\beta = 0$) is excluded with very high significance ($P > 99.99\%$). Lower luminosity ($P_{\rm r} \lesssim 10^{26}$ W/Hz), mostly FR I radio sources are known to display a much weaker cosmological evolution, which reaches $\approx$ zero at $P_{\rm r} < 10^{25}$ W/Hz (e.g. Gendre, Best & Wall 2010, and references therein). We took this into account by using the radio LFs of BL Lacs and FSRQs derived from those of FR Is and FR IIs and based on the beaming model of Urry & Padovani (1995), which agree well with those of recent blazar samples (Padovani et al. 2007; Giommi et al. 2009). We then used the fraction of beamed FR I blazars in bins of radio power to simulate the fraction of non-evolving radio sources as a function of power. This fraction is equal to 1 for $P_{\rm r} \leqslant 5 \times 10^{24}$ W/Hz, decreases monotonically with power, and reaches 0 for $P_{\rm r} \geqslant 5 \times 10^{27}$ W/Hz.

(iii) **Non-thermal component** To represent the non-thermal/jet component, we assume a simple homogeneous synchrotron self-Compton model (SSC, see, e.g. Tramacere et al. 2009, and references therein) with relativistic electrons distributed as a power law at low energies and as a log-parabola at high energies (Massaro et al. 2004, 2006). This model represents well the synchrotron part of the observed SEDs, which always extends at least to the optical band where the classification of blazars as FSRQs or BL Lacs occurs. As for the inverse Compton emission, which can be important in the soft X-ray band, we set the Compton dominance so as to reproduce the observed $f_{\rm x}/f_{\rm r}$ in FSRQs. This is sufficient for our purposes, since, complicating the emission with additional components, like thermal emission from accretion or inverse Compton on an external field of photons, would only modify somewhat the amount of observed soft X-rays in LSP blazars but would not change the composition of the samples, nor alter any of our conclusions.

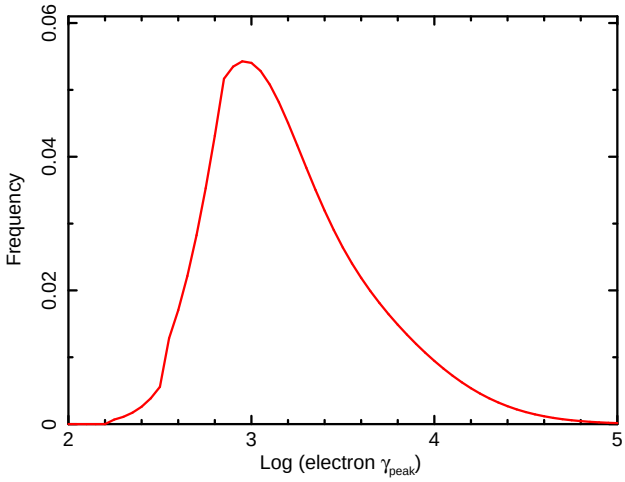

Figure 4. The distribution of the Lorentz factors of the electrons radiating at the peak of the synchrotron SED used for the simulation, which also assumes a magnetic field of B=0.15 Gauss and a gaussian distribution of Doppler factors with $\langle\delta\rangle$=15.

The Lorentz factors of the electrons radiating at the peak of the synchrotron SED component ($\gamma_{\rm peak}$) are distributed as shown in Fig. 4. The range of $\gamma_{\rm peak}$ ($\sim 2.5-4.5$) is that expected for typical parameters of the SSC model as shown in Fig. 36 of Abdo et al. (2010c). The particular shape of the distribution was chosen so as to empirically reproduce the observed $\nu^S_{\rm peak}$ distributions in radio and X-ray selected samples of blazars. The skewness to lower values is similar to that of the $f_{\rm x}/f_{\rm r}$ (a proxy for $\nu^S_{\rm peak}$) distribution adopted by Padovani & Giommi (1995) to unify X-ray selected and radio-selected BL Lacs. As regards the Doppler factor, we assumed a mean value of 15, which was chosen to be consistent with the mean superluminal speed $\beta_{\rm app} \sim 12$ obtained by Lister et al. (2009), and with the typical Lorentz factor $\Gamma \sim 15$ derived by Hovatta et al. (2009) (since for the angle that maximizes the apparent velocity $\delta \sim \beta_{\rm app} \sim \Gamma$).

(iv) **Accretion Disk and broad emission lines** We use the quasar spectral template of Vanden Berk et al. (2001), which has been built using an homogeneous dataset of over 2,200 SDSS spectra (see Fig. 4 of Giommi et al. 2011). A standard accretion disk is likely to be present only in so-called "high excitation" radio galaxies (HERGs), while it appears not to be there, or be less efficient, in low-excitation ones (LERGs). Almost all FR Is are LERGs, while most FR IIs are HERGs, although there is a population

of FR II LERGs as well. Chiaberge et al. (1999) and Donato et al. (2004) have in fact suggested that the obscuring torus, which is required by AGN unification schemes, is absent in FR Is, based on the high optical core detection rate and low X-ray intrinsic absorption, respectively. This would mean no accretion disk as well, otherwise one would see broad lines in their optical spectra, while, apart from a handful of objects (e.g. 3C 120), basically no FR I displays broad optical lines. Evans et al. (2006) have shown that the accretion flow luminosities of FR IIs are typically several orders of magnitude higher than those of FR Is. It then looks like LERGs, which means all FR Is and some FR IIs, either do not possess an accretion disk, or if the disk is present is much less efficient than in FR IIs (i.e. of the Advection Dominated Accretion Flow [ADAF] type). We have then associated the presence of a standard accretion disk only with beamed FR II sources and assumed that all those with an FR I parent (the non-evolving sources) have no disk (but see Section 6 for an alternative scenario).

(v) **Equivalent width distributions** The intrinsic (before dilution) distributions of the EW of the broad lines (Lyα, C IV, C III, Mg II, Hβ, Hα) have been assumed to be those of the radio quiet QSOs included in the SDSS database described in Section 3. We assumed Gaussian distributions characterized by the measured means ($\langle \mathrm{EW_{H\alpha}} \rangle$= 200 Å, $\langle \mathrm{EW_{H\beta}} \rangle$= 23 Å, $\langle \mathrm{EW_{Mg-II}} \rangle$= 18 Å, $\langle \mathrm{EW_{C-III}} \rangle$= 16 Å, $\langle \mathrm{EW_{C-IV}} \rangle$= 20 Å, $\langle \mathrm{EW_{Ly\alpha}} \rangle$= 47 Å) and dispersions for the various lines.

(vi) **The disk to jet power ratio** The disk and jet components in blazars are known to be correlated and possibly of the same order of magnitude, although there are uncertainties associated with estimating them (see, e.g. D'Elia, Padovani, & Landt 2003; Ghisellini et al. 2011). We are interested in the somewhat simpler question of determining how the luminosity of the accretion disk (blue bump intensity at 5000 Å) scales with radio power (at 5 GHz). The relevant data were derived by using the very large amount of multi-frequency information included in public databases and the tools that are now available to analyze SEDs (Stratta et al. 2011). Figure 1 gives some examples of representative objects. The amount of thermal flux in each FSRQ was estimated by matching the composite optical QSO spectrum of Vanden Berk et al. (2001) to the SED data in the blazar rest-frame. We have done that through a careful visual inspection of each SED and by adjusting the intensity of the composite QSO spectrum until it overlapped well to the observed emission. The use of this manual approach was necessary as the heterogeneity of the available data and flux variability does not allow the implementation of a robust automatic procedure. Fig. 1 gives examples of the matching of the composite QSO spectrum (blue line) to the data for the case of 3C273 or 3C279. In those objects where the available optical/UV data are limited to a magnitude in one or two colors, we matched the composite QSO spectrum to the flux level corresponding to the available magnitude(s), taking into account of redshift.

An upper limit was instead estimated for BL Lac objects by placing the composite QSO spectrum in the SED at an intensity such that the optical lines would not

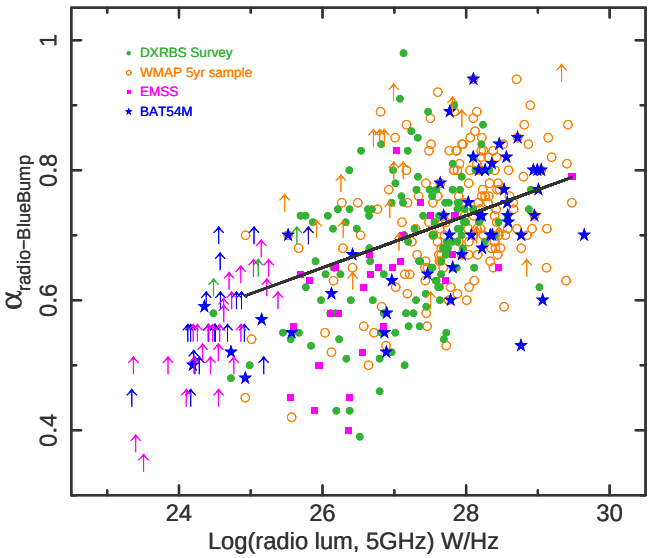

Figure 5. $\alpha_{r-BlueBump}$, the slope between the radio luminosity at 5 GHz (non-thermal boosted component) and the optical luminosity at 5000 Å due to the blue bump (thermal non-boosted component estimated from the blazars' SEDs as described in the text), is plotted against radio luminosity for a large number of blazars from several radio and X-ray selected samples. The solid line is the linear relationship used for our simulations (see text for details).

be detectable in the optical spectrum (typically a factor ten below the observed flux. Fig. 1 illustrates the case of MKN501). This was done for a large number of blazars selected in four surveys, two radio-selected (Deep X-ray Radio Blazar Sample [DXRBS] and WMAP5) and two X-ray selected (EMSS and *Swift*-BAT). The results are plotted in Fig. 5 where we can see that $\alpha_{r-BlueBump}$ (the slope between the 5 GHz luminosity and the blue bump intensity at 5000 Å and defined by $L_{\mathrm{disk}} = L_{\mathrm{r}}(\nu_{5000\mathrm{A}^{\circ}}/\nu_{5GHz})^{-\alpha_{\mathrm{r-BlueBump}}}$) correlates with radio luminosity, although with a large scatter. We interpret this as the result of relativistic beaming, in the sense that the larger the radio luminosity (and therefore the beaming amplification) the larger the ratio between non-thermal and thermal radiation.

We adopted a simple linear relationship between the two variables ($\alpha_{r-BlueBump} = 0.04$*$\log(\mathrm{L_{radio}}) - 0.39$, see Fig. 5) and assumed a Gaussian distribution around it with a dispersion of 0.1. This has been derived by fitting the WMAP5 and EMSS points in the Figure (see below). We did not take into account the lower limits on $\alpha_{r-BlueBump}$ since the large majority of them are at low radio power ($\lesssim 10^{26}$ W/Hz) and in our scenario these sources do not have a standard accretion disk.

(vii) **Host galaxy**

Following Scarpa et al. (2000) and Urry et al. (2000) we have assumed that the host galaxy of blazars is a giant elliptical with fixed absolute magnitude of $M_{\mathrm{R}} = -22.9$ as estimated by Sbarufatti, Treves, & Falomo (2005) using the same ΛCDM cosmology adopted in this paper. These authors have shown that the dispersion around this value is less than 1 magnitude and therefore such a giant elliptical galaxy can be considered a standard candle. For the spectral shape we used the galaxy tem-

plate of Mannucci et al. (2001), who derived it combining the data from 28 local elliptical galaxies observed in the wavelength range $0.12 - 2.4$ μm.

Figure 1 shows this template superposed to the SED of four well-known blazars.

4.2 Simulation steps

Our Monte Carlo simulations consist of the sequential execution of the following steps:

(i) draw a value for the radio luminosity and redshift of a simulated blazar based on the luminosity function and evolution described above;

(ii) draw a value of the Lorentz factor of the electron radiating at the peak of the synchrotron power ($\gamma_{\rm peak}$) from the distribution shown in Fig. 4, which is assumed to be independent of blazar luminosity;

(iii) Calculate the peak of the synchrotron power in the source rest frame. In our simulations we assume a simple SSC model, and therefore $\nu_{peak} = 3.2 \times 10^6 \gamma^2_{\rm peak} B\delta$. The value of $\gamma_{\rm peak}$ is derived in step ii), the magnetic field is fixed to B = 0.15 Gauss, and the Doppler factor δ is randomly drawn from a gaussian distribution with $\langle\delta\rangle = 15$ and $\sigma = 2$.

(iv) calculate the observed radio flux density (from the radio luminosity and redshift from step i)) and the non-thermal emission in the optical and X-ray bands under the assumption that the spectral shape of the observed emission is a log parabola around $\nu^S_{\rm peak}$ and that the low energy part of the SED (cm and mm wavelengths) is a power law, as is typically seen in blazars (see e.g. Fig. 1 for some representative examples, or Giommi et al. (2011) for a much larger sample of blazar SEDs);

(v) accept the source if its flux in the band under consideration (radio or X-ray) is above the flux limit chosen for the simulated survey;

(vi) add an accretion (blue bump) component as described above (only for beamed FR II sources), re-scaling the SDSS quasar template to this value;

(vii) draw a value of the equivalent width of Lyα, C IV, C III, Mg II, Hβ, Hα starting from the EW distribution observed in the SDSS radio quiet QSOs;

(viii) add the optical light of the host galaxy assuming a standard giant elliptical observed in blazars;

(ix) calculate the total optical light and the observed equivalent width of all the broad lines considered by taking into account the dilution due to the non-thermal and host galaxy optical light;

(x) classify the source as an FSRQ if the rest-frame EW of at least one of the broad lines that enter the optical band in the observer frame (which we assume to cover the $3,800 - 8,000$ Å range) is > 5 Å. Otherwise, the object is classified as a BL Lac, unless the host galaxy dominates the optical light causing the Ca H&K break to be larger than 0.4 (Marchã et al. 1996; Landt, Padovani, & Giommi 2002), in which case the source is classified as a radio galaxy. A BL Lac whose maximum EW is < 2 Å, or the non-thermal light is at least a factor 10 larger then that of the host galaxy (Piranomonte et al. 2007), is deemed to have a redshift which cannot be typically measured.

It is important to stress that the scope of our simulations is *not* to reproduce *all* the observational details. While that could be possible in theory, in practice it would require a large number of parameters and some speculations. Our approach is instead to keep the number of assumptions to a minimum, with the aim of allowing us to obtain robust, almost model-independent conclusions. Our main results are in fact independent of the simulation details (see Section 5.4).

4.3 Simulations of radio and X-ray surveys

We simulated a radio flux density limited survey with $f \geqslant 0.9$ Jy, to match the WMAP5 sample, and an X-ray flux limited survey down to 5×10^{-13} erg cm^{-2} s^{-1} in the $0.3 - 3.5$ keV band, in order to be able to compare it with the EMSS. To ensure good statistics each simulation run included 10,000 sources. In the X-ray case, since radio powers reach lower values than in the radio case, we extrapolated the radio LF down to 1.9×10^{23} W/Hz assuming the same slope.

5 COMPARING SIMULATIONS AND REAL DATA

In this section we make a detailed comparison between the results of our simulations and the observational data in terms of fractions of BL Lacs and FSRQs, redshift and $\nu^S_{\rm peak}$ distributions, and cosmological evolution using the $V/V_{\rm m}$ test (Schmidt 1968), where V is the volume out to the source and $V_{\rm m}$ is the the volume at the distance where the object would be at the flux limit. We also show where our simulated sources end up on the plot used by Fossati et al. (1998) when they first described the "blazar sequence".

5.1 Radio flux density limited survey

Table 1 summarizes our main results by giving the number of sources per class, their mean redshift, and $\langle V/V_{\rm m}\rangle$. The number in parenthesis refers to the BL Lacs with measurable redshift, to which the mean redshift and $\langle V/V_{\rm m}\rangle$ pertain. About 3/4 of our sources are classified as FSRQs, with the fraction of BL Lacs being $\sim 19.8\%$ of blazars, which is consistent with the value of $15.3^{+3.7}_{-3.0}\%$ in the WMAP5 sample (where the 1σ errors are based on binomial statistics: Gehrels 1986). A small fraction (5%) of the simulated blazars are classified as radio galaxies. These are bona-fide blazars misclassified because their non-thermal radiation is not strong enough to dilute the host galaxy component.

The mean redshift for our simulated FSRQs is in good agreement with the WMAP5 value of 1.13, while for BL Lacs this is slightly larger than the WMAP5 mean (0.55).

Fig.6 shows the overall good agreement between our simulated redshift distributions (where we have only included sources with a measurable redshift) and the observed ones.

63% of our BL Lacs have a redshift determination, in

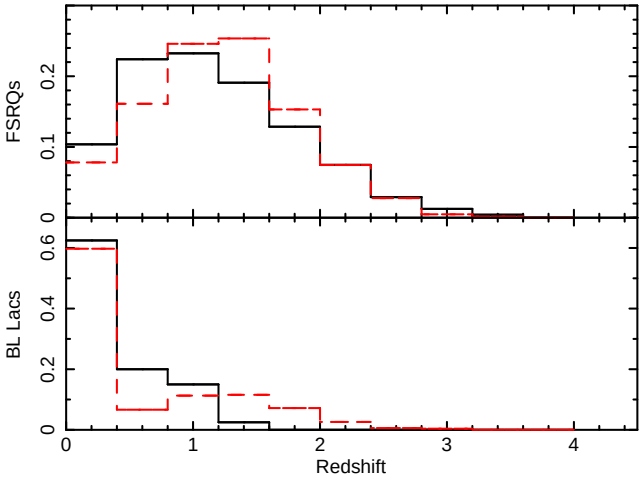

Figure 6. Top panel: the redshift distribution of the WMAP5 FSRQs (solid histogram) compared to that of FSRQs in a simulation of a radio survey (dashed histogram). Bottom panel: the redshift distribution of the WMAP5 BL Lacs (solid histogram) compared to that of BL Lacs in a simulation of a radio survey (dashed histogram)

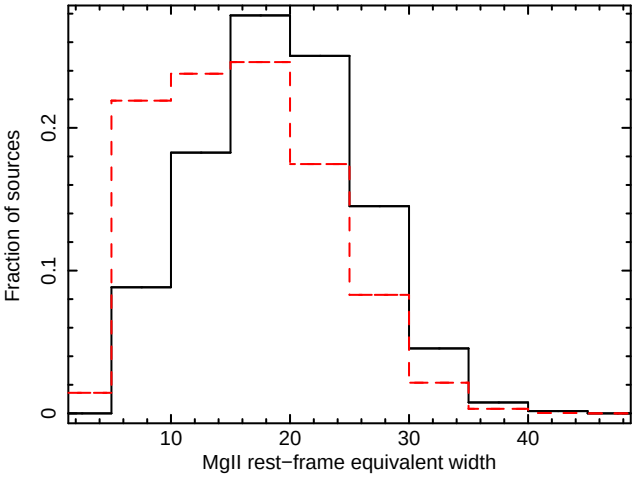

Figure 7. The Mg II EW distribution used as input for our simulation (solid line) and the output, diluted distribution for FSRQs (dashed line) in the simulated radio survey.

Table 1. Results from a simulation of a radio flux density limited survey (0.9 Jy)

Source type	Number of sources	$\langle z \rangle$	$\langle V/V_{\rm m} \rangle$
FSRQs	7,587	1.24	0.64
BL Lacs	1,879 (1,191)	0.87	0.60
Radio galaxies	534	0.04	0.48
Total	10,000	1.13	0.63

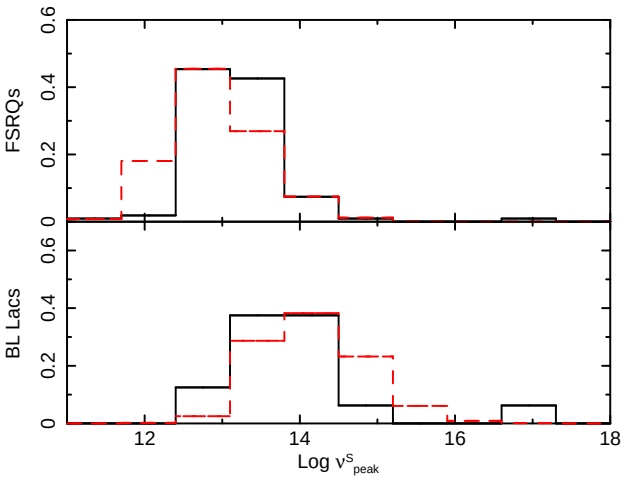

Figure 8. Top panel: the $\nu^S_{\rm peak}$ distribution of radio selected FSRQs taken from the work of Giommi et al. (2011) (solid histogram) compared to that of FSRQs in a simulation of a radio survey (dashed histogram). Bottom panel: the $\nu^S_{\rm peak}$ distribution of the BL Lacs in the radio sample of Giommi et al. (2011) (solid histogram) compared to that of BL Lacs in a simulation of a radio survey (dashed histogram).

excellent agreement with the WMAP5 value of 69^{+27}_{-20}%. 79% of the BL Lacs (68% of those with redshift) have a standard accretion disk and are therefore broad-lined but are classified as BL Lacs only because their observable emission lines are swamped by the non-thermal continuum.

As regards $\langle V/V_{\rm m} \rangle$, our simulated mean values agree with the observed ones of 0.62 ± 0.02 and 0.63 ± 0.05 for WMAP5 FSRQs and BL Lacs respectively (cf. also the value of 0.60 ± 0.05 for the 1 Jy BL Lac sample: Stickel et al. 1991).

Fig. 7 shows the EW distribution used as input for our simulation and the resulting one for FSRQs after the dilution due to the non-thermal and host galaxy components. The significant shift to lower values is clearly seen. This is similar to the comparison between real FSRQs and radio quiet QSOs shown in Fig. 3.

Fig. 8 compares the distributions of $\nu^S_{\rm peak}$, the synchrotron peak energy, of sources classified as FSRQs and BL Lacs in our simulation with those of blazars included the radio sample of Giommi et al. (2011), which is the sample with the best determination of $\nu^S_{\rm peak}$ values currently available. The agreement is clearly quite good and reproduces well the fact that BL Lacs tend to have $\nu^S_{\rm peak}$ values significantly higher than FSRQs.

We note that, although our input parameters were partly based on the WMAP5 sample, it is important to stress that, starting from a *single* LF and evolution, plus a fraction of non-evolving sources, we are able to reproduce quite well the main properties of the two blazar subclasses including those not part of the input (like relative fractions and percentage of BL Lacs with redshift).

5.2 X-ray flux limited survey

Table 2 summarizes our main results. About 2/3 of our blazars are classified as BL Lacs, which is consistent with the value of 73^{+19}_{-15}% in the EMSS sample. As in the radio case, a small fraction (15%) of the simulated blazars are misclassified as radio galaxies.

The mean redshifts for our simulated FSRQs and BL Lacs are in reasonable agreement with the EMSS blazar sample values ~ 1 and ~ 0.37. We note that, unlike the

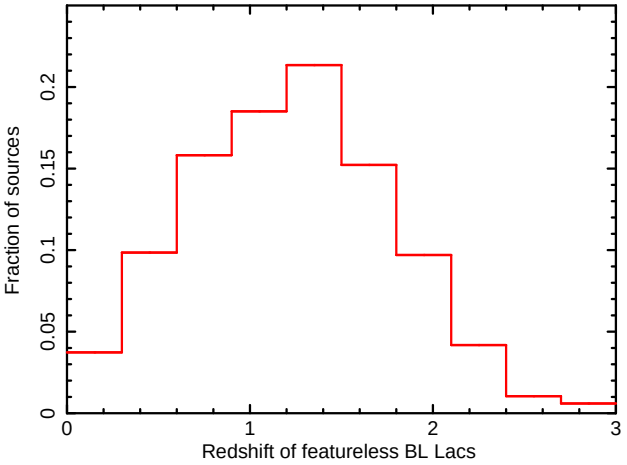

Figure 9. The redshift distribution of the BL Lacs that show a featureless spectrum in our simulation of a radio flux density limited survey, and that in a real survey would have no redshift determination.

Table 2. Results from a simulation of an X-ray flux limited survey (5×10^{-13} erg cm^{-2} s^{-1})

Source type	Number of sources	$\langle z \rangle$	$\langle V/V_{\rm m} \rangle$
FSRQs	2,836	1.23	0.65
BL Lacs (all)	5,622 (4,460)	0.36	0.51
BL Lacs (log $\nu^S_{\rm peak} > 16.5$)	927 (895)	0.33	0.45
BL Lacs (log $\nu^S_{\rm peak} > 17$)	185 (177)	0.34	0.34
Radio galaxies	1,542	0.04	0.48
Total	10,000	0.58	0.55

WMAP5 sample, the EMSS sample is relatively small (56 sources) and therefore a detailed comparison is hampered by the small number statistics.

79% of our BL Lacs have a redshift determination, in good agreement with the EMSS value of 93^{+26}_{-21}%. Although we assumed that all non-evolving sources do not have a standard accretion disk, 30% of the BL Lacs possess one and are classified as BL Lacs only because their emission lines are swamped by the non-thermal continuum. The smaller fraction of X-ray selected BL Lacs with disks in our simulations, as compared to radio-selected ones, is in accordance with the fact that fewer EMSS BL Lacs have emission lines clearly detectable in their optical spectra than, for example, 1 Jy BL Lacs (see, e.g. Rector et al. 2000; Rector & Stocke 2001; Stickel, Fried, & Kühr 1993).

As regards $V/V_{\rm m}$, our simulated mean values agree reasonably well with the EMSS ones of 0.67 ± 0.08 and 0.42 ± 0.05 for FSRQs and BL Lacs respectively, derived using the samples described in Padovani et al. (2003).

Fig. 10 compares the distributions of $\nu^S_{\rm peak}$ of FSRQs and BL Lacs in our simulation with those of blazars belonging to the soft X-ray sample of Giommi et al. (2011), which includes *Planck*, *Swift* and *Fermi* observed blazars and it is therefore probably the sample with the best determination of $\nu^S_{\rm peak}$ values currently available. The agreement is clearly good reproducing well the fact that BL Lacs have much higher $\nu^S_{\rm peak}$ values than FSRQs.

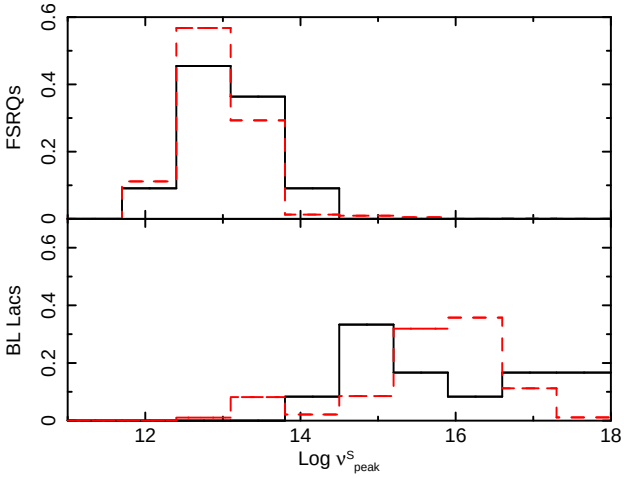

Figure 10. Top panel: the $\nu^S_{\rm peak}$ distribution of the X-ray selected FSRQs in Giommi et al. (2011) (solid histogram) compared to that of FSRQs in a simulation of an X-ray survey (dashed histogram). Bottom panel: the $\nu^S_{\rm peak}$ distribution of the BL Lacs in the X-ray flux limited sample of Giommi et al. (2011) (solid histogram) compared to that of BL Lacs in a simulation of an X-ray survey (dashed histogram).

5.3 A blazar sequence?

The existence of a strong anti-correlation between bolometric luminosity and $\nu^S_{\rm peak}$, known as the "blazar sequence" has been the subject of intense discussions since its first proposal by Fossati et al. (1998) and Ghisellini et al. (1998) (e.g., Giommi, Menna & Padovani 1999; Padovani et al. 2003; Caccianiga & Marchã 2004; Nieppola et al. 2006; Padovani 2007; Ghisellini & Tavecchio 2008; Nieppola et al. 2008; Giommi et al. 2011). In this section we use our simulations to comment on the existence of such a sequence.

Figure 11 shows our radio and X-ray selected simulated blazars in the $\log(\nu^S_{\rm peak})$ – $\log(\nu L_\nu(5\ {\rm GHz}))$ plane. This reproduces the famous plot used by Fossati et al. (1998) to propose the existence of the blazar sequence based on the correlation shown in this plane by FSRQs and BL Lacs discovered in shallow radio surveys (2 and 1 Jy samples) and BL Lacs found in the X-ray flux limited *Einstein* slew survey ($f_{\rm x} \gtrsim 10^{-12}$erg cm^{-2} s^{-1}). Indeed, considered together the simulated radio and X-ray selected blazars display a broad correlation with radio selected FSRQs and BL Lacs (red open squares and open circles) mostly filling the top left and central part of the diagram and X-ray selected BL Lacs (green open circles) mostly confined to the lower right corner of the plot. This particular positioning of the points (bright FSRQs of the LSP type vs. fainter HSP BL Lacs) is not due to any intrinsic correlation between luminosity and $\nu^S_{\rm peak}$ but is instead the result of a selection effect resulting from the fact that bright radio sources are mostly drawn from the high end of the blazar luminosity function, while BL Lacs in X-ray flux limited samples are mostly high $\nu^S_{\rm peak}$ sources

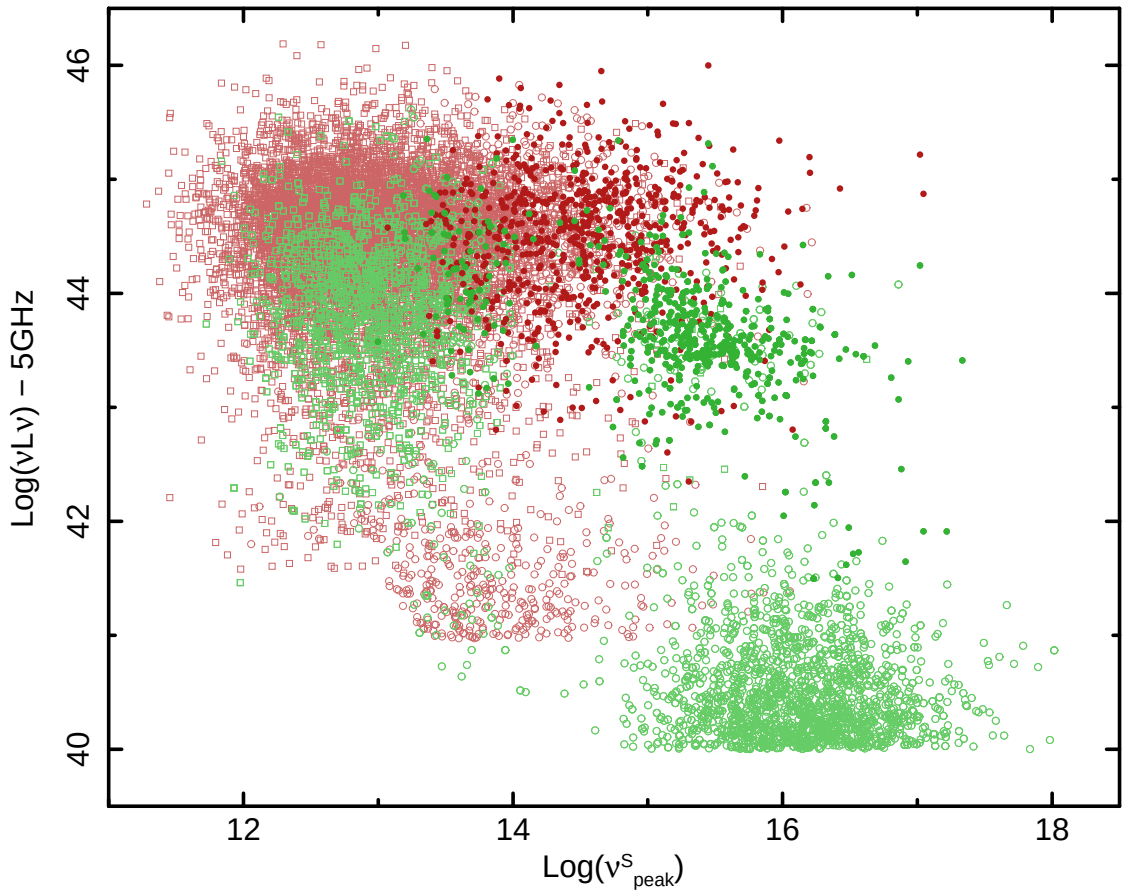

Figure 11. The FSRQs (open squares) and BL Lacs (circles) of our radio flux density limited ($f_{\rm r} > 0.9$ Jy, red symbols) and X-ray flux limited ($f_{\rm x} > 5 \times 10^{-13}$erg cm^{-2} s^{-1} , green symbols) simulated samples, plotted in the log(ν)-log(νL$_\nu$) plane, the portion of the parameter space used by Fossati et al. (1998) to show the existence of the "blazar sequence" by comparing radio ($f_{\rm r} > 1 - 2$ Jy) and X-ray selected ($f_{\rm x} \gtrsim 10^{-12}$erg cm^{-2} s^{-1}) complete samples. Filled circles represent BL Lacs with very weak lines (EW < 2 Å) or completely featureless which, in a real survey would most probably not have a measured redshift, and therefore would not appear in the plot. Note that almost all of these objects occupy the top right part of the diagram. Blazars in this area are high-luminosity HSP sources, that is objects that are "forbidden" in the blazar sequence scenario.

(intrinsically rare) drawn from the low end of the luminosity function where the source density is largest. The most important difference between Fig. 11 and the diagram of Fossati et al. (1998) is in the high-luminosity - high $\nu^S_{\rm peak}$ part, where most of the radio and X-ray selected objects with no redshift (red and green filled points) are located. These sources could not be plotted by Fossati et al. (1998) since the luminosity of blazars without redshift cannot be estimated. This left the top right part of the Fossati et al. (1998) diagram empty, thus contributing to make the displayed data look like a power sequence.

5.4 Assessing the stability of our results

To assess the dependence of our results on the adopted LF and evolution, we have made the following two checks: first, we varied their input values by 1σ adopting $\Phi(P) \propto P^{-2.85}$, $k = 7.0$, and $\beta = -1.4$ (luminosity peak at $z \sim 1.9$) and $\Phi(P) \propto P^{-3.1}$, $k = 7.7$, and $\beta = -1.7$ (luminosity peak at $z \sim 1.75$); second, we used as an alternative LF the sum of the BL Lac and FSRQ LFs based on the beaming model of Urry & Padovani (1995) (converted to $H_0 = 70$ km s^{-1} Mpc^{-1}) assuming, for consistency with the way they were derived, a pure luminosity evolution of the type $P(z) = P(0)\exp[T(z)/\tau]$, where $T(z)$ is the look-back time. A value of $\tau = 0.33$, which is consistent with the evolution of DXRBS FSRQs and BL Lacs combined (based on the samples in Padovani et al. 2007), was also assumed.

We have also checked the dependence of our results on the assumed value of the Doppler factor, running the simulation with values of $\langle\delta\rangle$ ranging from 5 to 20, and we have also considered the case of a dependence of δ on radio power as suggested by some authors (e.g. Hovatta et al. 2009), although Lister et al. (2009), who studied a complete sample, have not been able to confirm such a correlation.

In all cases our main results, that is the prevalence of FSRQs and BL Lacs in radio and X-ray selected samples respectively, the higher redshifts and evolution of FSRQs as compared to BL Lacs, and the no evolution of X-ray selected BL Lacs, were confirmed, which shows that they are independent of the details of the LF and evolution.

We also modified our assumption that standard accretion disks are associated only with sources having an

FR II parent but the simulations we obtained were inconsistent with observations. In fact, even if the relatively small fraction of 20% of objects with FR I parents are randomly assigned an accretion disk and allowed to evolve, X-ray selected BL Lacs reach too high values of $\langle V/V_{\rm m}\rangle$ and $\langle z\rangle$, 0.58 and 0.91 respectively, which are incompatible with observations.

6 DISCUSSION

So far, blazars have been largely discovered in the radio, μ-wave, X-ray or γ-ray bands. We have shown that the wide diversity of $\nu^S_{\rm peak}$ observed in blazars results in strong differences in the observed flux at radio or X-ray frequencies (up to three orders of magnitudes) causing severe selection effects in surveys performed in these energy bands. This, combined with the fact that blazars are always identified on the basis of their optical spectrum, which reflects a mix of non-thermal, thermal, and host galaxy emission, has been the origin of a number of enduring open issues about the nature of blazars.

6.1 Evolution

A long-standing blazar puzzle is the difference in redshift distribution and cosmological evolution between FSRQs and BL Lacs, selected both in the radio and in the X-ray band. BL Lacs are mostly located at low redshifts and exhibit moderate, or even negative, evolution, while FSRQs evolve strongly just like radio quiet QSOs and show a redshift distribution that peaks at $z > 1$ (Stocke et al. 1982; Stickel et al. 1991; Rector et al. 2000; Beckmann et al. 2003; Padovani et al. 2007; Giommi et al. 2009). Our simulations reproduce quite well both of these findings (see Fig. 6 and Tables 1 and 2) implying that they are due to heavy selection effects. Most of the simulated BL Lacs found in radio surveys are luminous objects with broad lines that are diluted by non-thermal radiation beyond the 5 Å EW limit (many of them just below, thus allowing a measurement of their redshift), while the BL Lacs found in simulated X-ray surveys typically show high $\nu^S_{\rm peak}$ values (and therefore are X-ray bright) and are drawn from the low-power end of the radio luminosity function where non-evolving FR Is are preferentially found (Section 4.1). We note that the $\langle V/V_{\rm m}\rangle$ of radio selected BL Lacs is not too different from that of FSRQs, while the $\langle V/V_{\rm m}\rangle$ of X-ray selected BL Lacs is significantly lower, as found in real surveys (Section 5.1).

Another interesting outcome of our simulations is the fact that X-ray selected BL Lacs with progressively larger values of $\nu^S_{\rm peak}$ are characterized by lower and lower values of $\langle V/V_{\rm m}\rangle$ (see Tab. 2). This is in full agreement with the puzzling, and so far unexplained, results of Rector et al. (2000) and of Giommi, Menna & Padovani (1999) who reported that the $\langle V/V_{\rm m}\rangle$ of BL Lacs is a function of their X-ray-to-radio flux ratio.

6.2 $\nu^S_{\rm peak}$ distribution

Recent results, based on radio and γ-ray surveys, have revealed that BL Lacs, on average, display a distribution of $\nu^S_{\rm peak}$ energies, which is shifted to values higher than those of FSRQs (Abdo et al. 2010c; Giommi et al. 2011), expanding on the well-known fact that high $\nu^S_{\rm peak}$ objects (HSPs) are always BL Lacs. This experimental difference is well reproduced in our simulations (see Fig. 8) which give $\langle\log(\nu^S_{\rm peak})\rangle = 12.9$ for FSRQs and $\langle\log(\nu^S_{\rm peak})\rangle = 14.1$ for BL Lacs for the case of a radio survey. This distinction is due to the fact that blazars with higher $\nu^S_{\rm peak}$ values produce more non-thermal optical light than low $\nu^S_{\rm peak}$ sources, diluting more easily the broad line component, and are therefore classified more frequently as BL Lac objects. We note that this has been interpreted in the literature as an intrinsic physical difference between LSP (detected mostly in the radio band) and HSP (detected mostly in the X-ray and γ-ray band) blazars due to the fact that HSPs are observationally characterized by a low intrinsic power and external radiation field, given their very weak or absent emission lines. As a consequence, cooling was thought to be less dramatic in HSP allowing particles to reach energies high enough to produce synchrotron emission well into the X-ray band (Ghisellini et al. 1998). In our scenario, instead, all sources have exactly the same chance of being HSP or LSP (that is, the value of $\gamma_{\rm peak}$ is drawn from the distribution shown in Fig. 4 *independently* of luminosity) and the very different $\nu^S_{\rm peak}$ distributions observed in radio and X-ray surveys arise from the strong selection effect discussed in Section 5.3 and the emission line dilution mentioned above.

Our simulations predict the existence of a significant number of BL Lacs with redshift that cannot be measured, which occurs when both $\nu^S_{\rm peak}$ and radio power are so large that dilution becomes extreme. For example, $\sim 81\%$ of our simulated sources with $\nu^S_{\rm peak} > 10^{15}$ Hz and $P_{\rm r} > 10^{26}$ W/Hz have no redshift. This is consistent with the fact that most BL Lacs in current γ-ray selected samples have no measured redshift, as *Fermi* is known to preferentially select high $\nu^S_{\rm peak}$ BL Lacs (Abdo et al. 2010a, 2011b). This effect is also clearly shown in Fig. 11 where most of the simulated blazars with no measurable redshift (filled circles with light colors) occupy the top right part of the diagram. Fig. 9 shows the intrinsic redshift distribution of these featureless BL Lacs for the case of our simulation of a radio flux density limited survey.

6.3 What is a BL Lac?

Blandford & Rees (1978) had originally suggested that the absence of broad lines in BL Lacs was due to a very bright, Doppler-boosted synchrotron continuum. In the years following that paper observations of various BL Lacs, mostly selected in the X-ray band, showed that in many cases their optical spectrum was not swamped by a non-thermal component, as host galaxy features were very visible, and it was thought that most BL Lacs had intrinsically weak lines. We have shown here that these two possibilities are not mutually exclusive and indeed are both viable, depending on radio power and, therefore, on the band of selection. One important consequence of our scenario is that objects so far classified as BL Lacs on the basis of their *observed* weak, or unde-

tectable, emission lines belong to two physically different classes: intrinsically weak lined objects, whose parents are LERGs/FR Is (more common in X-ray selected samples, since they reach lower radio powers) and heavily diluted broad-lined sources, which are beamed HERGs/FR IIs (more frequent in radio selected samples). Therefore, while the non-thermal engine is probably the same, the thermal one is obviously different. This solves at once the issue of the FSRQ/BL Lac transition objects and of the many differences between BL Lacs selected in the radio and X-ray bands, which include line strength, extended radio emission and morphology, and evolution (e.g. Rector & Stocke 2001, and references therein). This hypothesis, which explains also many other open issues of blazar research, is directly testable. Our simulations, in fact, imply that the majority of sources in high-flux density radio-selected samples are identified as BL Lacs only because all lines have EW $<$ 5 Å *in the optical observing window*. These sources should show a strong (EW $>$ 5 Å) Hα line if observed in the near or mid-infrared, since this is the strongest emission line, and would then be considered FSRQs, which reinforces our point on the very strong effect that line dilution has on blazar classification. HERG/FR II BL Lacs, then, should be easily recognizable through infrared spectroscopy. These sources, as expected, are also more dominant at higher radio powers: for example, according to our radio simulation the fraction of BL Lacs with standard accretion disks is only $\sim$ 3% for $P_{\rm r} \leqslant 10^{26}$ W/Hz but becomes $\sim$ 98% above this value. This also means that fainter radio-selected samples of BL Lacs should be more and more similar to X-ray selected ones, apart from their $\nu^S_{\rm peak}$ values, since higher $\nu^S_{\rm peak}$ are easier to detect in the X-rays (Padovani & Giommi 1995).

The implications of our hypothesis for unified schemes is quite straightforward: the parent population of BL Lacs need to include both LERGs/FR Is and HERGs/FR IIs, while that of FSRQs is made up of HERGs/FR IIs only. This should have only a small effect, for example, on the LF fitting done by Urry & Padovani (1995), as HERG/FR II BL Lacs make up the high-power end of the radio LF while most of the number density comes from LERG/FR I BL Lacs.

6.4 Blazar classification

Our new scenario has strong implications on blazar classification as well. If the relevant physical distinction for radio sources is between LERGs (mostly FR Is) and HERGs (FR IIs), for most purposes then (LFs, evolution, etc.) HERG/FR II BL Lacs should be simply grouped with FSRQs. How does one distinguish in practice HERG/FR II BL Lacs from LERG/FR I BL Lacs? This is simple in the presence of *any* (even weak) broad lines or for transition objects. In other cases (e.g. completely featureless spectrum or in presence of absorption features) there is no easy way to distinguish between the two subclasses although, for example, radio power and/or morphology could help. Given the paucity of known LERG/FR Is at relative high redshifts, X-ray selected (and also fainter radio-selected) BL Lac samples are also useful in selecting such sources, which are very relevant also for the study of the so-called "AGN feedback" and the role that AGN radio emission plays in galaxy evolution through the so-called "radio-mode" accretion (Croton et al. 2006). It should also be clear that BL Lacs can be used to study the broader issue of the relationship between LERGs and HERGs, including their evolution.

A by-product of our simulations has also been the realization that some sources classified as radio-galaxies do *not* have their jets oriented at large angles with respect to the line of sight, as expected, but are instead moderately beamed blazars with their non-thermal emission swamped by the galaxy (note that none of these objects has a standard accretion disk). These sources, which are all local ($\sim$ 90% at $z \leqslant 0.07$) should be recognizable by their blazar-like SEDs and indeed some of them have already been identified by Dennett-Thorpe & Marchã (2000), Giommi et al. (2002, 2005) and Antón & Browne (2005).

Recently Ghisellini et al. (2011) have proposed a new classification scheme to divide BL Lacs from FSRQs, which is based on the broad line region (BLR) luminosity in Eddington units and set at a dividing value of $L_{\rm BLR}/L_{\rm Edd} \sim 5 \times 10^{-4}$. This turns out to be also the value, which separates radiatively efficient (i.e., standard accretion disks) from radiatively inefficient (i.e., ADAFs) regimes, and therefore coincides with our HERG/FR II – LERG/FR I division. Therefore, Ghisellini et al. (2011) are also suggesting that HERG/FR II BL Lacs belong with the FSRQs.

7 CONCLUSIONS

We have tackled the open issue of the relationship between the various blazar subclasses, and of the consequences of selection effects, through extensive Monte Carlo simulations. Our approach is based on robust observational input, and on various results obtained by many authors over the past 20 years or so, which had never before been put together in a comprehensive way. We kept the number of assumptions and parameters to a minimum so as to draw robust conclusions. Our starting point are two populations of high-excitation, high radio-power, evolving and low-excitation, low-power, non-evolving radio sources. To these we add: an homogeneous synchrotron self-Compton component with a distribution of electron Lorentz factors peaked at relatively low values, an optical/UV quasar template, the EW distributions of the main broad lines observed in radio-quiet quasars, a distribution of disk/jet ratios, and finally an elliptical host galaxy.

Our main results can be summarized as follows:

(1) we explain the main properties of all blazar subclasses, namely FSRQs and BL Lacs selected in the radio and X-ray band. Our simulations reproduce well the prevalence of FSRQs and BL Lacs in radio and X-ray selected samples respectively, the higher redshifts, evolution and lower $\nu^S_{\rm peak}$ of FSRQs as compared to BL Lacs, the non evolution of X-ray selected BL Lacs, and the main differences between radio and X-ray-selected BL Lacs in

a manner that does not dependent significantly on the adopted LF and evolutionary details;

(2) objects classified until now as BL Lacs on the basis of their *observed* weak, or undetectable, emission lines actually belong to two physically different classes: most BL Lacs in high flux density, radio-selected samples are actually beamed radio quasars with their emission lines heavily diluted by the non-thermal continuum and for all purposes should then be grouped with FSRQs. Infrared spectroscopy should reveal in many such sources the presence of strong (EW > 5 Å) Hα; most BL Lacs selected in the X-ray band are instead intrinsically weak-lined, low-excitation radio galaxies with a strong non-thermal, jet component;

(3) there are only two main intrinsic blazar types: low-ionization (mostly beamed FR Is) and high-ionization (beamed FR IIs) ones. All other classifications and classes proposed so far are not physically relevant and are simply due to severe selection effects and different relative strengths of the non-thermal, thermal, and galaxy components, which make up blazars' optical emission;

(4) some sources classified as radio-galaxies on the basis of their optical properties are instead moderately beamed blazars (that is, sources with their jets forming a small angle with respect to the line of sight) with their non-thermal emission swamped by the host galaxy. Some of these sources have already been recognized from their SEDs;

(5) our simulations show that the purported correlation between luminosity and $\nu^S_{\rm peak}$, the so-called "blazar sequence", is likely a selection effect resulting from comparing shallow radio surveys with shallow X-ray surveys. We also show that blazars with featureless optical spectra, and therefore without a redshift determination, are mostly high luminosity – high $\nu^S_{\rm peak}$ sources, a type of blazar that should not exist in the "blazar sequence" scenario. This is consistent with the lack of redshift in the majority of BL Lacs in current γ-ray selected samples, as *Fermi* is known to preferentially select high $\nu^S_{\rm peak}$ BL Lacs;

(6) the topics addressed in this paper are not relevant only to blazars but are also related to the broader issues of low-ionization radio galaxies and radio-mode "AGN feedback".

In this paper we limited our simulations to the radio and the X-ray bands where SSC is a fair approximation of the observed non-thermal emission. The properties of γ-ray detected blazars are instead not consistent with simple SSC models (e.g. Abdo et al. 2010c), and almost half of the radio and X-ray selected LSP blazars are γ-ray quiet (e.g. Giommi et al. 2011). The present approach must therefore be integrated with additional information about the properties of the inverse Compton emission before it can be used to simulate γ-ray surveys. We are planning to extend our simulations to the γ-ray band by taking into account the recent results of Giommi et al. (2011) who determined the γ-ray properties of blazar samples selected in different bands.

ACKNOWLEDGMENTS

We thank A. Pollock for careful reading of the manuscript and useful suggestions. ST would like to thank Mark Subbarao and Rich Plotkin for useful discussions on the SDSS spectroscopic pipeline. We also thank Matteo Perri for providing part of the software used for our Monte Carlo simulations. We acknowledge the use of data and software facilities from the ASI Science Data Center (ASDC), managed by the Italian Space Agency (ASI). Part of this work is based on archival data and on bibliographic information obtained from the NASA/IPAC Extragalactic Database (NED) and from the Astrophysics Data System (ADS). Funding for the SDSS and SDSS-II was provided by the Alfred P. Sloan Foundation, the Participating Institutions, the National Science Foundation, the U.S. Department of Energy, the National Aeronautics and Space Administration, the Japanese Monbukagakusho, the Max Planck Society, and the Higher Education Funding Council for England. The SDSS was managed by the Astrophysical Research Consortium for the Participating Institutions.

REFERENCES

Abdo A. A., et al., 2010a, ApJ, 715, 429
Abdo A. A., et al., 2010b, ApJS, 188, 405
Abdo A. A., et al., 2010c, ApJ, 716, 30
Abdo A. A., et al., 2011, submitted to ApJ, (arXiv:1108.1435)
Ackermann M., et al., 2011, submitted to ApJ, (arXiv:1108.1420)
Ajello M., et al., 2009, ApJ, 699, 603
Antón S., Browne I. W. A., 2005, MNRAS, 356, 225
Baldwin J. A., 1977, ApJ, 214, 679
Blandford R. D., Rees M. J., 1978, in Pittsburg Conference on BL Lac Objects, Ed. A. M. Wolfe, Pittsburgh, University of Pittsburgh press, p. 328
Beckmann V., Engels D., Bade N., Wucknitz O, 2003, A&A, 401, 927
Capetti A., Raiteri C. M., Buttiglione S., 2010, A&A, 516, A59
Caccianiga A., Marchã M. J., MNRAS, 348, 937
Chiaberge M., Capetti A., Celotti A., 1999, A&A, 349, 77
Croton D. J., et al., 2006, MNRAS, 365, 11
Dennett-Thorpe J., Marchã M. J., 2000, A&A, 361, 480
D'Elia V., Padovani P., Landt H., 2003, MNRAS, 339, 1081
Donato D., Sambruna R. M., Gliozzi M., 2004, ApJ, 617, 915
Evans D. A., Worrall D. M., Hardcastle M. J., Kraft R. P., Birkinshaw M., 2006, ApJ, 642, 96
Fossati G., Maraschi L., Celotti A., Comastri A., Ghisellini G., 1998 MNRAS, 299, 433
Francis P. J., Hooper E. J., Impey C. D., 1993, AJ, 106, 417
Gehrels N., 1986, ApJ, 303, 336
Gendre M. A., Best P. N., Wall J. V., 2010, MNRAS, 450, 1719

Ghisellini G., Celotti A., Fossati G., Maraschi L., Comastri A., 1998, MNRAS, 301, 451
Ghisellin G., & Tavecchio F., 2008, MNRAS, 387, 1669
Ghisellini G., Tavecchio F., Foschini L., Ghirlanda G., 2011, MNRAS, 414, 2674
Giommi P., Menna M.T., Padovani, P., 1999, MNRAS, 310, 465
Giommi P., Piranomonte, S., Perri, M., Padovani, P., 2005, AA&A, 434, 385
Giommi P., Perri M., Piranomonte S., Padovani P., 2002, Blazar Astrophysics with BeppoSAX and Other Observatories, Eds. P. Giommi, E. Massaro, G. Palumbo, ESA-ESRIN, 2002, p. 123
Giommi P., Capalbi M., Cavazzuti E., et al., 2007, A&A, 468, 571
Giommi P., Colafrancesco S., Padovani P., Gasparrini D., Cavazzuti E., Cutini S., 2009, A&A, 508, 107
Giommi P., et al., 2011, A&A, submitted, ArXiv:1108.1114
Hovatta T., Valtaoja E., Tornikoski M., Lähteenmäki A., 2009, A&A, 494, 527
Kimball A. E., Ivezić Ž., Wiita P. J., Schneider D. P., 2011, AJ, 141, 182
Kollgaard R. I., Wardle J. F. C., Roberts D. H., Gabuzda D. C., 1992, AJ, 104, 1687
Komatsu E., et al., 2011, ApJS, 192, 18
Landt H., Padovani P., Giommi P., 2002, MNRAS, 336, 945
Lister M. L., et al., 2009, AJ, 138, 1874
Mannucci F., Basile F., Poggianti B. M., Cimatti A., Daddi E., Pozzetti L., Vanzi L., 2001, MNRAS, 326, 745
Marchã M. J. M., Browne I. W. A., Impey C. D., Smith P. S., 1996, MNRAS, 281, 425
Massaro E., Perri, M., Giommi, P., Nesci, R., 2004, A&A, 413, 489
Massaro E., Tramacere, A., Perri, M., Giommi, P., Tosti, G.., 2006, A&A, 448, 861
Massaro E., Giommi P., Leto C., Marchegiani P., Maselli A., Perri M., Piranomonte S., Sclavi S., 2009, A&A, 495, 691
Massaro E., Giommi P., Leto C., Marchegiani P., Maselli A., Perri M., Piranomonte S., 2011, in preparation
Nieppola E., Tornikoski M., & Valatoja E., 2006, A&A, 445, 441
Nieppola E., Valatoja E., Tornikoski M., Hovatta T., Kotiranta M., 2008, A&A, 488, 867
Padovani, Perlman E. S., Landt H., Giommi P., Perri M., 2003, ApJ, 588, 128
Padovani P., Giommi P., 1995, ApJ, 444, 567
Padovani P., Giommi P., Landt H., Perlman E. S., 2007, ApJ, 662, 198
Padovani P., Miller N., Kellermann K. I., Mainieri V., Rosati P., Tozzi P., 2011, ApJ, in press
Padovani P., Perlman E. S., Landt H., Giommi P., Perri M., 2003, ApJ, 588, 128
Padovani P., 2007, Ap&SS, 309, 63
Pian E., et al., 1999, ApJ, 521, 112
Piranomonte S., Perri M., Giommi P., Landt H., Padovani P., 2007, A&A, 470, 787
Planck Collaboration, 2011, A&A, in press (arXiv:1101.2041)
Plotkin R. M., et al., 2010, AJ, 139, 390
Rector T. A., Stocke J. T., Perlman E. S., Morris S. L., Gioia I. M., 2000, AJ, 120, 1626
Rector T. A., Stocke J. T., 2001, AJ, 122, 565
Sbarufatti B., Treves A., Falomo R., 2005, ApJ, 635, 173
Scarpa R., Falomo R., 1997, A&A, 325, 109
Scarpa R., Urry C. M., Falomo R., Pesce J. E., Treves A., 2000, ApJ, 532, 740
Schmidt M., 1968, ApJ, 151, 393
Shaw M. S., Romani R. W., Healey S. E., Cotter G., Michelson P. F., Readhead A. C. S., 2009, ApJ, 704, 477
Shaw M. S., Romani R. W., Cotter G., Readhead A. C. S., Healey S. E., Michelson P. F., Fermi LAT Collaboration, 2010, AAS, 42, #434.12
Stickel M., Fried J. W., Kühr H., 1993, A&AS, 98, 393
Stickel M., Padovani P., Urry C. M., Fried J. W., Kühr H., 1991, ApJ, 374, 431
Stocke J. T., Liebert J., Stockman H., Danziger J., Lub J., Maccacaro T., Griffiths R., Giommi P., 1982, MNRAS, 200, 27
Stocke J. T., Morris S. L., Gioia I. M., Maccacaro T., Schild R., Wolter A., Fleming T. A., Henry J. P., 1991, ApJS, 76, 813
Stratta G., Capalbi M., Giommi P., Primavera R., Cutini S., Gasparrini D., 2011, ArXiv:1103.0749
Tramacere A., Giommi P., Perri M., Verrecchia F., Tosti G., 2009, A&A, 501, 879
Turriziani S., 2010, Ph.D. Thesis
Turriziani S., 2011, AAS, 43, #125.03
Urry C. M., Padovani P., 1995, PASP, 107, 803
Urry C. M., Scarpa R., O'Dowd M., Falomo R., Pesce J. E., Treves A., 2000, ApJ, 532, 816
Vanden Berk, D. E., et al., 2001, AJ, 122, 549
Vermeulen R. C., Taylor, G. B., Readhead A. C. S., Browne, I. W. A., AJ 111, 1013
Wall J. V., Jackson C. A., Shaver P. A., Hook I. M., Kellermann K. I., 2005, A&A, 434, 133
Wall J. V., Pope A., Scott D., 2008, MNRAS, 383, 435
Wright E. L., et al., 2009, ApJS, 180, 283